APL Materials

RESEARCH ARTICLE | JUNE 16 2026

Time-resolved magnetic force microscopy of all-optical magnetization switching

Special Collection: Ultrafast Opto-Spintronics

Dinar Khusyainov ✉ ; Rein Liefferink ; Fabian Kammerbauer ; Robert Frömter ; Mathias Kläui ; Dmitry Kozodaev ; Johan H. Mentink ; Dmytro Afanasiev ; Theo Rasing ; Alexey Kimel

APL Mater. 14, 061109 (2026)
https://doi.org/10.1063/5.0336534

Time-resolved magnetic force microscopy of all-optical magnetization switching

Cite as: APL Mater. 14, 061109 (2026); doi: 10.1063/5.0336534
Submitted: 31 March 2026 • Accepted: 30 May 2026 •
Published Online: 16 June 2026

Dinar Khusyainov,[1,a] Rein Liefferink,[1] Fabian Kammerbauer,[2] Robert Frömter,[2] Mathias Kläui,[2] Dmitry Kozodaev,[3] Johan H. Mentink,[1] Dmytro Afanasiev,[1] Theo Rasing,[1] and Alexey Kimel[1]

AFFILIATIONS

[1] Radboud University, Institute for Molecules and Materials, Nijmegen 6525, AJ, Netherlands
[2] Institute of Physics, Johannes Gutenberg University Mainz, Mainz 55099, Germany
[3] NT-MDT BV, Sutton 11A, Apeldoorn 7327, AB, Netherlands

Note: This paper is part of the Special Topic on Ultrafast Opto-Spintronics.
[a] **Author to whom correspondence should be addressed:** dinar.khusyainov@ru.nl

ABSTRACT

Understanding spin dynamics at ever shorter time and smaller length scales is one of the major challenges in fundamental and applied magnetism, leading in particular to the discovery of giant magnetoresistance and All-Optical Switching (AOS) of magnetization and motivating the development of large-scale facilities such as x-ray free-electron lasers. Here, we propose a conceptually distinct approach to explore ultrafast laser-induced spin dynamics at the nanoscale by combining tabletop Magnetic Force Microscopy (MFM) with femtosecond laser excitation. By writing magnetic domains not with a single but with a pair of mutually delayed ultrashort laser pulses, we observe the spin dynamics by analyzing the final static nanotextured domain pattern as a function of pump-to-pump delay. We show that using MFM, we are able to deduce not only the average reversed magnetization but also the switched areas of nanoscale domains with picosecond temporal resolution. The capabilities of the technique are further demonstrated by applying it to study ultrafast helicity-dependent AOS of magnetization in ferromagnetic Pt/Co/Pt, where magnetization can be reversed with a pair of 100-fs and 3-ps laser pulses. Tracking the laser-induced area of the nanotextured domains as a function of the time separation between the pump pulses reveals critical slowing down of the spin dynamics near the Curie temperature of Co, thereby increasing the efficiency of dual-pulse AOS.

INTRODUCTION

Over the past five decades, the focus on progress in fundamental and applied condensed matter physics can be summarized in two words: *smaller* and *faster*. Magnetism is no exception. Interest in ultrafast magnetic phenomena at the nanoscale has been continuously driven by the potential of this research to shape the future of magnetic data storage.[1–4] This motivation has long fueled the development of advanced experimental techniques capable of probing spin dynamics with nanometer spatial resolution and picosecond temporal resolution.[5,6] Magnetic recording achieved via All-Optical Switching (AOS), which relies solely on light without external magnetic fields, is one of the phenomena whose understanding greatly benefited from such studies.[7–15]

Here, we demonstrate the capability of a tabletop scanning-probe method to perform *in situ* investigations of ultrafast laser-induced spin dynamics at the nanoscale. The main idea of this approach is to study ultrafast laser-induced processes using not one but two or more ultrashort laser excitation pulses.[16–20] By employing pulses of different widths and varying the delays between them, information about ultrafast laser-induced spin dynamics can be deduced by analyzing the final nanoscale domain patterns using the submicrometer resolution of intrinsically slow Magnetic Force Microscopy (MFM).[21–24]

The power of this approach is demonstrated by its application to the problem of helicity-dependent all-optical switching (HD-AOS) in the ferromagnetic heterostructure Pt/Co/Pt. Using HD-AOS, many (~100) circularly polarized picosecond pulses are

required to switch magnetization through the magnetic circular dichroism effect.[10–12,15,25,26] Recent studies by K. Yamada *et al.*[20,27] have shown that a combination of two pulses separated on a ps timescale dramatically reduces the number of laser pulses required to achieve multipulse HD-AOS in this ferromagnetic material. In these studies, a short, linearly polarized 100-fs pulse was employed to excite the magnetic system far from equilibrium, followed by a circularly polarized 3-ps pulse that triggered homogeneous magnetization reversal. These experiments used a magneto-optical detection method that constrained the resolution to the optical diffraction limit and, therefore, depended on macroscopic parameters such as average magnetization. Furthermore, our recent study combining MFM with short laser pulses demonstrated how stochasticity and domain nanotexture affect HD-AOS.[15] Here, we show that using MFM to examine dual-laser-pulse magnetization reversal allows us to explore both the microscopic and macroscopic characteristics of laser-induced nanotextured magnetic domains, studying the switched area as well as average magnetization. We vary the temporal separation between the two pump pulses and examine the nanotextured domains induced by each pair. Using three-temperature modeling (3TM), we find that the dependence of the switched area of the reversed nanotextured domains on pulse-to-pulse separation correlates with the spin-temperature relaxation. To reproduce the experimentally observed dependence of the average magnetization and switched area of reversed nanotextured domains as a function of time separation between the excitation pulses requires accounting for the critical anomaly of the spin heat capacity near the Curie temperature of Co. Analyzing the dynamics of the temperature relaxation of the spin system, we observe that a 3 ps long pulse forces the magnetic system to spend more time in a highly non-equilibrium state by exploiting critical slowing down of spins, resulting in a higher efficiency of dual-pulse and multipulse AOS.

RESULTS

We use a multilayer structure with perpendicular magnetic anisotropy, consisting of thin films of Ta (1.0 nm)/MgO (2.0 nm)/Pt (3.0 nm)/Co (0.6 nm)/Pt (3.0 nm)/Ta (4.0 nm) deposited on a synthetic glass substrate. The sample exhibits perpendicular magnetic anisotropy, with an out-of-plane magnetic hysteresis loop and a coercive field of 28 mT (see supplementary material 1 and Methods). To measure the nanotextured features of the laser-induced magnetic domains, we use MFM coupled with a femtosecond laser source, as shown in Fig. 1(a) (see Methods). For dual-pulse excitation, we split the laser beam with a beam splitter and send one beam through a delay line. Another pulse is stretched to 3 ps using a glass rod pulse stretcher (NewLightPhotonics N-SF11). The second pulse duration is 100 fs. The polarization of both pulses is controlled using a

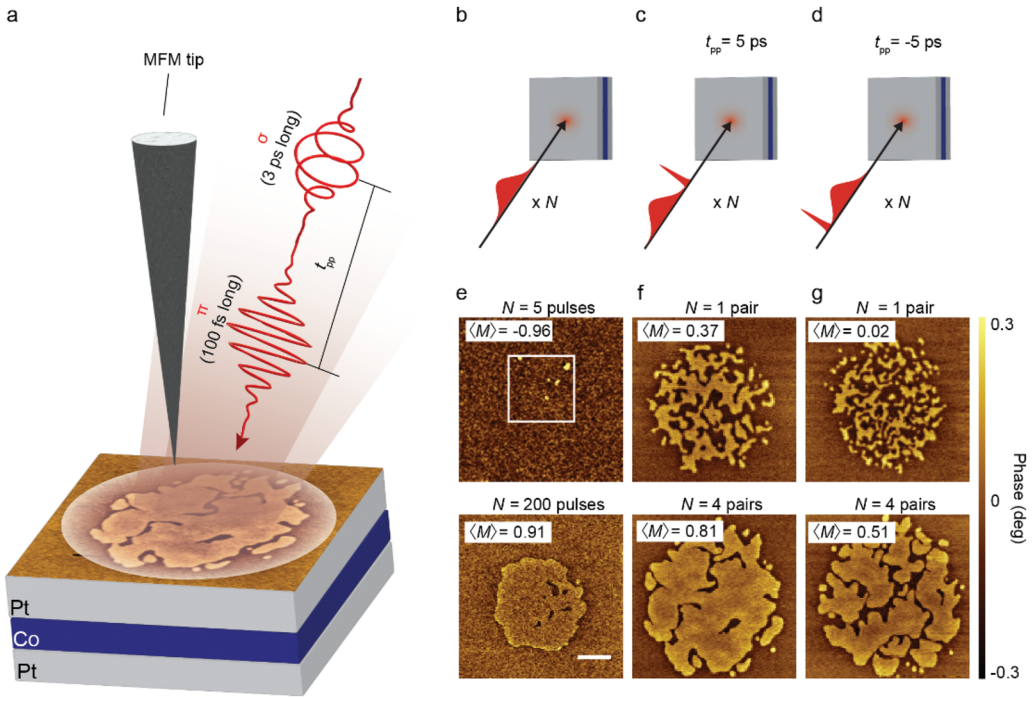

FIG. 1. Dual-pulse excitation and MFM probing. (a) Sketch of the experimental setup. We utilize a magnetic force microscope (MFM) coupled with a source of dual-pulse laser excitation of a Pt/Co/Pt system. We use 100-fs linearly (π) and 3-ps circularly polarized (σ) laser pulses. (b) Single pulse excitation geometry. In this geometry, we use a single or a sequence of 3 ps σ laser pulses with a separation time of 2 ms. (c) Dual-pulse excitation geometry of the experiment. We use a pair of π and σ laser pulses with a separation time t_{pp} = 5 ps. (d) Dual-pulse excitation geometry with $t_{pp} = -5$ ps. (e) MFM images of the nucleated domains after a sequence of the σ laser pulses. We present MFM images after excitation with 5 and 200 pulses. We calculate the average magnetization within the white square of size 10 × 10 μm^2. The scale bar is 5 μm. (f) MFM images obtained after dual-pulse excitation at t_{pp} = 5 ps. (g) MFM images obtained after dual-pulse excitation at $t_{pp} = -5$ ps. We present MFM images after excitation with one pair of pulses and a sequence of 4 pairs of pulses separated by 2 ms.

half-wave plate and a quarter-wave plate. The two beams are coupled through a beamsplitter and focused on the sample's surface. Using a delay line, we can control the time separation between the two pulses with a time step of ~1 ps (see supplementary material 2). We nucleate magnetic domains via an ultrafast demagnetization process[1] and immediately measure them *in situ* using the retractable scanning MFM head. For a 3-ps laser pulse, we used a fluence of F_{ps} = 1.9 mJ/cm^2, which is required for HD-AOS.[15] For a 100 fs laser pulse, we used a fluence of F_{fs} = 0.8 mJ/cm^2 to keep the temperature of the magnetic system below the nucleation threshold while maintaining approximately the same peak spin temperature as for a 3 ps pulse (see supplementary material 3).

First, to analyze the laser-induced nanotextured domains, we use a macroscopic parameter, the average magnetization $\langle M \rangle$, which was previously used in magneto-optics. We calculate $\langle M \rangle$ within a white square of size 10 × 10 μm^2.[27] When $\langle M \rangle = -1$, all spins inside

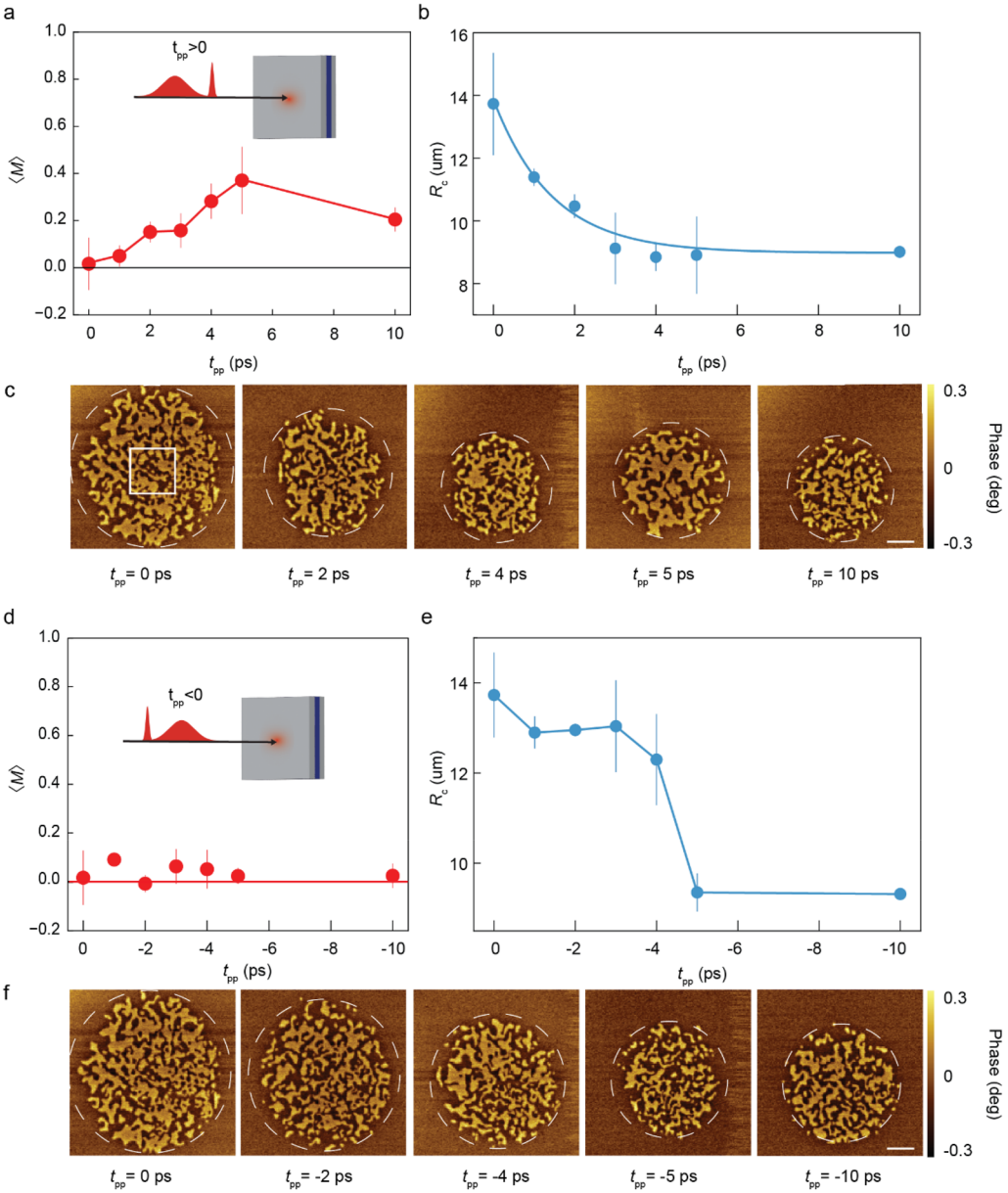

FIG. 2. Ultrafast spin dynamics revealed by a ps–fs pulse pair and MFM probing. (a) and (d) Average magnetization and (b) and (e) radius of area of laser-induced domains as a function of positive and negative pulse separation t_{pp}, respectively. The inset shows the excitation geometry. Line in b(e) is an exponential fit (guide to the eye), respectively. (c) and (f) MFM images of the laser-induced domains using dual-pulse excitation as a function of the positive and negative t_{pp}, respectively. The white dashed circle on the MFM images serves to highlight the radius change of the laser-induced domain area. The size of the MFM images is 30 × 30 μm^2. The scale bar is 5 μm.

the box are "down," whereas $\langle M \rangle = 1$ indicates that the laser has homogeneously switched all spins from magnetization "down" to "up."

We begin by examining the effect of a single 3-ps circularly polarized pulse [Fig. 1(b)] starting from a homogeneously magnetized sample with $\langle M \rangle = -1$. A sequence of five such pulses, separated by 2 ms, nucleates small magnetic domains with diameters of ~1 μm that are randomly distributed across the illuminated region, resulting in an average magnetization of $\langle M \rangle = -0.96$. Achieving homogeneous magnetization reversal with this single-pulse excitation geometry requires hundreds of pulses;[10–12,28] using 200 pulses at a fluence F_{ps} yields $\langle M \rangle = 0.91$ [Fig. 1(e)].

We next investigate dual-pulse excitation [Fig. 1(c)]. Figure 1(f) shows the MFM images obtained using a pulse pair consisting of a 100 fs linearly and a 3 ps circularly polarized pulse, separated by $t_{pp} = 5$ ps. A single pulse pair produces only partial switching ($\langle M \rangle = 0.37$), but applying four pulse pairs separated by 2 ms significantly improves the average magnetization to $\langle M \rangle = 0.81$. When we reverse the order of the pulses [Fig. 1(d)], the average magnetization drops: one reversed-order pair yields almost no net reversal ($\langle M \rangle = 0.02$), and four such pairs produce only moderate switching ($\langle M \rangle = 0.51$), as shown in Fig. 1(g). To investigate how the time separation affects the switching and provides access to ultrafast spin dynamics, we next study laser-induced domain nucleation as a function of t_{pp}.

We first focus on positive time separation, i.e., the ps pulse arrives after the fs one. Figure 2(c) shows MFM images of the laser-induced nanotextured domains as a function of positive t_{pp}. Since the laser-induced domain formation process is stochastic, we performed the experiment three times for each t_{pp}. The corresponding average magnetization [Fig. 2(a)] increases with t_{pp}, peaks at ~0.4 for $t_{pp} = 5$ ps, and then decreases to ~0.2 at $t_{pp} = 10$ ps, in agreement with earlier observations.[27] We then reverse the pulse order and repeat the delay-dependent measurement in Fig. 2(f). For negative delays, the average magnetization remains essentially zero for all t_{pp} [Fig. 2(d)], indicating that this macroscopic parameter carries no dynamical information.

MFM offers significantly higher spatial resolution than magneto-optical microscopy, enabling us to resolve small nanotextured domains that were previously inaccessible, along with their microscopic changes. Subsequently, in Figs. 2(c) and 2(f), we observe that the area containing laser-induced domains is strongly dependent on the time separation t_{pp}. To highlight this, we fit the laser-induced domains within a circle (dashed line in Figs. 2(c) and 2(f)) and plot the radius of this circle (R_c) in Figs. 2(b) and 2(e) for positive and negative values of t_{pp}, respectively. The radius of the laser-induced magnetic domains is extracted from MFM phase images using a fixed contrast threshold, and the radius of the grains is estimated by treating them as a single grain.

We plot R_c as a function of positive t_{pp} in Fig. 2(b). We see that the R_c decreases exponentially as a function of t_{pp} from 14 to 9 μm within the range of t_{pp} from 0 to 4 ps and remains stable at 9 μm in the range of t_{pp} from 4 to 10 ps. We fit this dependence with an exponential decay function [see the solid line in Fig. 2(b)] and extract a characteristic time constant of 1.5 ± 0.3 ps, a clear indication of the ultrafast dynamics. Next, we plot R_c as a function of negative t_{pp} in Fig. 2(e). Unlike the positive-delay case, R_c demonstrates distinct dynamics on t_{pp}. Initially, R_c remains constant at a value of 14 μm in the range of t_{pp} from 0 to −3 ps, followed by relaxation of R_c from 14 to 9 μm in the range of t_{pp} from −3 to −5 ps, and finally remains stable at 9 μm from −5 to −10 ps. A simple exponential decay cannot capture this behavior, which differs qualitatively from the dynamics observed in Fig. 2(b). As the initial plateau lasts longer than the long pulse itself, this suggests that an additional physical mechanism influences the thermal relaxation of the spin system. To identify the origin of this anomalously slow relaxation, we turn to three-temperature-model simulations.

DISCUSSION

We first identify the relation of the radius R_c to the ultrafast spin temperature dynamics. The radius R_c represents the boundary of the region where the local laser fluence exceeds the critical threshold F_c required to induce nanoscale domains. Because the laser pulse has a Gaussian spatial profile, the deposited energy—and, therefore, the temperature rise—is highest at the beam center and decays radially outward. As the peak incidence fluence F increases, the region where $F(r) \geq F_c$ expands, where r is the radius of the Gaussian beam, defining a circular area where we observe laser-induced domains with radius R_c. This R_c is therefore directly related to the experimentally observed size of the switched area after the laser pulse. The threshold fluence F_c reflects the minimum energy needed to reach the temperature required for domain nucleation. As the peak fluence increases, the region where the local temperature exceeds the switching threshold expands, leading to logarithmic growth of the switched area with fluence. We demonstrate the relation between R_c and fluence in supplementary material 4.

The existence of a sharp nucleation threshold suggests a thermally activated process. In particular, experiments[15] and modeling[29] show that the nucleation process is thermally activated and that the probability of domain formation follows an Arrhenius-type temperature dependence. A simple Arrhenius process with a constant energy barrier does not fully capture this behavior; instead, it yields a smoother transition. This is because the temperature dependence of the magnetic free energy cannot be ignored here, being especially strong near the phase transition due to fluctuations.[29] Including this will produce a strong threshold. When this strong temperature dependence is combined with the spatial fluence profile of the laser beam, it results in an apparent sharp threshold fluence and a well-defined switching radius. Given this relation, we solve the 3TM to relate experimental data of R_c on t_{pp} to ultrafast spin temperature dynamics. We would like to note that we do not include explicit lateral or vertical heat diffusion. This approximation is justified because the effects discussed in this study occur on a 10-ps timescale, where the dominant processes are local electron, spin, and lattice energy exchange rather than spatial heat transport (see supplementary material 5).

A three-temperature model is commonly employed to simulate relaxation in a ferromagnetic metallic system, tracking the temperature changes of three baths—electrons, lattice, and spins—over time, following laser pulse excitation.[3,12,30,31] The model uses three coupled differential equations

$$C_e(T_e)\frac{dT_e}{dt} = -G_{el}(T_e - T_l) - G_{es}(T_e - T_s) + P_{ps}(t - t_{pp}, r) + P_{fs}(t, r), \quad (1)$$

$$C_l(T_l)\frac{dT_l}{dt} = -G_{el}(T_l - T_e) - G_{sl}(T_l - T_s), \quad (2)$$

$$C_s(T_s)\frac{dT_s}{dt} = -G_{es}(T_s - T_e) - G_{sl}(T_s - T_l), \quad (3)$$

where T_e, T_l, and T_s are the electron, lattice, and spin temperatures; C_e is the electronic heat capacity, modeled as γT_e; C_l is the lattice heat capacity, which linearly depends on temperature; G_{el}, G_{es}, and G_{sl} are the electron–phonon, electron–spin, and spin–lattice coupling constants; and $P_{ps}(t - t_{pp}, r)$ and $P_{fs}(t, r)$ are the absorbed temporal and spatial laser power densities for the 3 ps and 100 fs pulses, respectively. We calculate the absorbed fluence in the sample in supplementary material 3. The parameters for the 3TM are listed in supplementary material 6, which presents the averaged values for the Pt/Co/Pt stack. Note that Ta and MgO are not considered.

We focus on the spin temperature for two reasons: (1) the electronic system relaxes on sub-picosecond timescales after laser excitation with a 100 fs pulse and, therefore, cannot account for the observed ps dynamics (see supplementary material 3 and Ref. 12); (2) With MFM, we are sensitive only to the spin system of our sample, while ultrafast magneto-optical measurements usually rely on a change in the dielectric tensor of the material (which can also be affected by electrons or lattice contributions). We solve the 3TM model using Eqs. (1)–(3) using parameters from the experiment and extract the peak spin temperature as a function of r and t_{pp}. Given the nucleation threshold fluence F_c from the experiment and the spatial full width at half maximum of the two beams (see Methods), we can calculate R_c, at which the spin temperature T_s reaches its peak at the fluence F_c (see supplementary material 7). We plot the calculated R_c as a function of t_{pp} in Figs. 3(a) and 3(b) (gray lines) and compare them with the experimental data. We can see that for positive values of t_{pp} [Fig. 3(a)], the calculated R_c captures the dynamical behavior of R_c on t_{pp} in the experiment, but it is off by around a factor of 3 for the R_c values. However, for negative t_{pp} values [Fig. 3(b)], the calculated R_c does not agree with either the dynamical behavior of R_c on t_{pp} or with the values of R_c in the experiment. To reproduce the experimental results in our model, we need to account for additional physical effects that modify the magnetic system's dynamical response.

According to the 3TM model (see supplementary material 3), the spin peak temperature during single pulse illumination reaches T_c of our film (T_c~500K[32]). The effect that typically impacts the dynamics of magnetic systems near T_c is a critical slowing down of spin dynamics, usually due to critical behavior of the heat capacity in the vicinity of T_c.[33–36] To phenomenologically capture this behavior within the three-temperature model, we introduce a temperature-dependent spin heat capacity using a phenomenological function consisting of a constant background contribution and a critical anomaly centered at T_c,[37]

$$C_s(T_s) = C_{s0}\left(1 + \frac{\varsigma}{1 + \left|\frac{T - T_c}{\Delta}\right|^{\alpha}}\right), \quad (4)$$

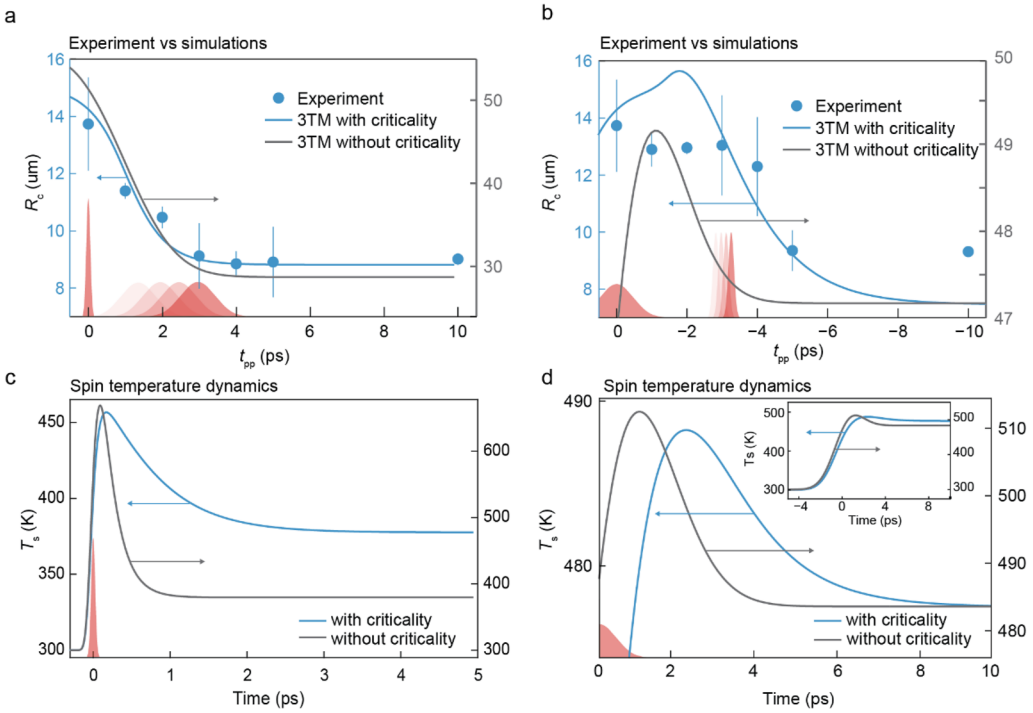

FIG. 3. Ultrafast spin temperature relaxation dynamics. (a) and (b) Radius R_c as a function of positive (a) and negative (b) t_{pp} values. We compare simulation vs experiment (solid line vs data points). We plot data points and simulations with criticality on the left axis, while simulations without including criticality on the right axis. (c) and (d) Ultrafast spin temperature dynamics initiated by a single fs (c) and ps pulse (d).

where $C_{s0} = 4 \cdot 10^4$ J/m^{3}K,[30] Δ is the width of the criticality region, taken to be equal to 5 K,[33] and ς and α are fitting parameters representing the amplitude and scaling of criticality in the heat capacity.

Next, we calculate R_c as a function of t_{pp}, taking into account Eq. (4) in our 3 TM simulations. We plot R_c as a function of t_{pp} in Figs. 3(a) and 3(b) (blue line). We can see that for positive t_{pp} values, the dynamics and the R_c values agree well with experimental data. For negative t_{pp}, we see that R_c now captures the dynamical properties of the plateau before the relaxation, followed by relaxation, and matches the experimentally observed R_c values quantitatively. The best agreement is obtained for a criticality amplitude of $\varsigma = 24.9$ and $\alpha = 0.7$ in the spin heat capacity (4) (supplementary material 8). The estimated value of the spin heat capacity out of equilibrium (at $T_s = 500$ K) is close to the values previously reported for a thin Ni film out of equilibrium[38] and similar to the total equilibrium heat capacity of a Co/Pt multilayer at room temperature.[39] However, the extracted value of the critical exponent of heat capacity is larger than the recently reported value of $\alpha = 0.07$[38] from photoemission spectroscopy experiments for a Ni thin film and the theoretical values for the 3D Ising and 3D Heisenberg models ($\alpha \sim 0.1$)[34]. Consequently, the fitted exponent should be interpreted as an effective phenomenological parameter for our sample that describes the sharpness of the heat-capacity anomaly, rather than the universal equilibrium critical exponent.

Using the extracted 3TM model parameters, we can plot the spin-temperature dynamics initiated by the first pulse in the pair in the center of the laser beam. We plot the fs pulse-initiated spin-temperature dynamics in Fig. 3(c). We compare the spin-temperature dynamics for two cases: with criticality in the spin heat capacity and without. We fit the spin temperature relaxation dynamics to an exponential decay function and extract the characteristic time constants. We can see that without criticality, the spin temperature relaxes with different characteristic time constants. Indeed, fitting the decay shows a characteristic time constant of $\tau_{fs} = 216 \pm 1$ fs, while including criticality, the time constant becomes $\tau_{fs,cr} = 805 \pm 6$ fs, demonstrating a substantial slowing down of the relaxation of the spin temperature by up to a factor of 4. In Fig. 3(d), we plot the dynamics of the spin temperature initiated by a ps pulse, including and excluding the critical phenomena in the spin heat capacity. First, we see that the spin temperature reaches its peak after excitation with the ps pulse at ~1 ps without criticality and at ~3 ps with criticality. This delay in reaching peak spin temperature aligns well with the experimentally observed plateau in the dependence of R_c on t_{pp}. We can see that the relaxation of the spin temperature also differs between the two cases. We fit the relaxation of the spin temperature using an exponential decay function. The extracted characteristic time constants are $\tau_{ps} = 925 \pm 8$ fs and $\tau_{ps,cr} = 1647 \pm 7$ fs. This demonstrates that criticality in the spin heat capacity substantially slows down the ultrafast spin-temperature relaxation dynamics.

Increasing the temperature relaxation time using ps laser pulses and operating near T_c affects the size of the laser-induced domains, as we illustrate in supplementary material 9. Here, for single pulse excitation, we observe that the longer the spin-temperature relaxation after excitation, the larger the average size of the domains. This size dependence might also be related to criticality and possibly explain why ps-long pulses are more efficient for HD-AOS.[12] Moreover, as the temperature approaches the Curie temperature, the growth of the spin–spin correlation length is expected near a second-order phase transition. As a result, fluctuations become correlated over larger spatial regions, leading to the formation of large domains of aligned or reversed spins. This growth of correlated domains underlies the phenomenon of critical slowing down: because increasingly large regions must reorganize collectively, the relaxation time grows strongly near the critical point. Consequently, the longer the system is maintained in the critical fluctuation regime, the larger these fluctuating domains can become.[40] Similar results were observed experimentally under equilibrium conditions, as the size of the nucleated magnetic domains with magnetic pulses increased with increasing temperature in Co/Pt.[41] This may indicate that the magnetic system in Co/Pt still partially maintains its equilibrium properties even under the non-equilibrium conditions of a ps pulse.

Finally, we discuss why the average magnetization is higher when a short 100-fs pulse precedes the 3-ps pulse. Using atomistic spin dynamics, K. Yamada *et al.*[27] demonstrated that a 100-fs laser pulse triggers the formation of nanometer-scale magnetic domains, appearing ~4 ps after exposure. As shown in supplementary material 10, when the 100-fs pulse excites the magnetic system first, the following relaxation of the spin temperature allows the magnetic system to cool by ~50 K before the 3-ps pulse arrives at $t_{pp} = 4$ ps, enabling the formation of nanotextured domains. The subsequent 3-ps pulse brings the magnetic system to T_c, exploiting critical slowing down and reversing the remaining unswitched magnetization through enhanced magnetic circular dichroism near nanotextured domains.[15] By contrast, when the 3-ps pulse arrives first, the system cannot cool efficiently on a picosecond timescale and remains near T_c, postponing formation of nanotextured domains. The following 100-fs pulse then drives the system above T_c, producing only small domains and leaving the average magnetization close to zero. Direct visualization of nanoscale domain formation on ultrafast timescales remains challenging because of its inherent stochasticity and requires further measures to improve. However, dual-pulse excitation and MFM *in situ* probing offer new perspectives for studying such processes.

CONCLUSION

In this study, we have investigated all-optical magnetization switching in ferromagnetic Pt/Co/Pt film using a dual-pulse excitation scheme combined with *in situ* magnetic force microscopy. By probing the laser-induced magnetic domains with an MFM, we access macroscopic switching parameters that are usually captured by conventional macroscopic magneto-optical observables, such as average magnetization, but now with nanoscale spatial resolution. We demonstrate that the radius of the switched area of laser-induced domains provides a sensitive measure of ultrafast spin relaxation processes initiated by the first pulse in a pulse pair. While the average magnetization shows little or no dependence on pulse separation in certain excitation geometries, the radius of the switched area reveals clear delay-dependent signatures of spin-temperature relaxation on picosecond timescales. By comparing the experimentally extracted radius of the switched area with a three-temperature-model simulation of this radius, we show that the observed delay dependence can be consistently interpreted in terms of ultrafast spin-temperature

relaxation. In particular, the relaxation dynamics exhibit an anomalous slowing down that cannot be reproduced without accounting for the critical behavior of the spin heat capacity near the Curie temperature. This criticality slows down the ultrafast spin temperature relaxation by up to a factor of 4. This critical slowing down prolongs the residence time of the spin system in a highly non-equilibrium state, thereby increasing the average size of the laser-induced domains and subsequently enhancing the efficiency of subsequent magnetization reversal. Our measurements demonstrate that dual-pulse excitation and MFM probing are powerful techniques for measuring ultrafast spin-relaxation dynamics and HD-AOS in magnetic systems with nanoscale spatial and ps resolution. Beyond the investigation of all-optical switching in ferromagnetic thin films with perpendicular magnetic anisotropy, the presented dual-excitation ultrafast MFM approach offers a versatile platform for studying a broader range of nanoscale magnetization dynamics. In particular, the combination of nanometer spatial resolution with dual-pulse excitations enables future studies of nucleation dynamics of skyrmions[42,43] or even exotic merons in in-plane magnetic films.[44]

METHODS

Sample

We used a multilayer structure with a perpendicular magnetic anisotropy, consisting of thin films of Ta (1.0 nm), MgO (2.0 nm), Pt (3.0 nm), Co (0.6 nm), Pt (3.0 nm), and Ta (4.0 nm) deposited on a synthetic glass substrate. Magnetic properties were characterized using a Faraday rotation setup by measuring the out-of-plane hysteresis loop. The structure shows a coercive field of about 28 mT.

Laser excitation

An amplified Ti:sapphire laser system (Spectra-Physics Spitfire Ace) with a central wavelength of 800 nm, adjustable pulse durations of 100 femtoseconds, and a repetition rate of 1 kHz was employed to locally manipulate the magnetization of the sample surface. A quarter-wave plate was utilized to adjust the helicity of the laser pulses, while an external Pockels cell was employed to control the number of pulses during sequential illumination. We measured the FWHM of the fs-pulse and ps-beam spots to be ~90 and ~110 μm, respectively, using the knife-edge method. The experimental fluence values provided in the main text correspond to the incident fluence at the sample surface. For the 3 TM simulations, we used the absorbed fluence (see supplementary material 3). The pulse widths of the ps and fs pulses were measured with a Spectra-Physics PulseScout, defining the pulse duration at FWHM.

MFM

We utilized an NT-MDT NTEGRA atomic force microscope for the MFM measurements. MFM images were acquired with a probe height of less than 100 nm. The two-pass MFM method was used. Low-moment MFM tips (NT-MDT MFM LM) were utilized to avoid disturbing the magnetic domains in Pt/Co/Pt. MFM images were corrected using the median line correction method. The quantity measured with MFM is a phase shift, proportional to the second derivative of the out-of-plane component of the stray magnetic field:[22] $\Delta\theta \propto \partial^2 H_{sz}/\partial z^2$, where H_{sz} is the out-of-plane component of the stray magnetic field and z is the tip–sample direction.

SUPPLEMENTARY MATERIAL

See the supplementary material for further sample characterization details, which include the magnetic out-of-plane hysteresis loop, the domain nucleation threshold induced by a single laser pulse, and how pulse width affects laser-induced domain formation. In addition, we provide parameters for 3 TM simulations, such as the absorption profile, electron, lattice, and spin temperature dynamics triggered by single and dual-pulse excitation, as well as the lateral spin temperature distribution and spin heat capacity criticality used in these simulations.

ACKNOWLEDGMENTS

The authors acknowledge K. Saeedi and C. Berkhout for their technical support. This study was funded by ERC Grant No. 485 101078206 ASTRAL, the European Union Horizon 2020 and innovation program under the European Research Council ERC Grant Agreement No. 856538 (3D-MAGiC), and the Gravitation program of the Dutch Ministry of Education, Culture and Science (OCW) under the research program "Materials for the Quantum Age" (QuMat) Registration No. 024.005.006. The group in Mainz acknowledges financial support from the Deutsche Forschungsgemeinschaft (DFG, German Research Foundation) SFB TRR 173 Spin + X (Project Nos. A01, B02, A12, and B12 #268565370, TRR 288 Elasto-Q-Mat (Project A12) No. #422213477, and the Horizon Europe Project No. 101070290 (NIMFEIA), as well as TopDyn.

AUTHOR DECLARATIONS

Conflict of Interest

The authors have no conflicts to disclose.

Author Contributions

Dinar Khusyainov: Conceptualization (equal); Data curation (lead); Formal analysis (lead); Investigation (lead); Methodology (lead); Validation (lead); Visualization (lead); Writing – original draft (lead); Writing – review & editing (lead). **Rein Liefferink**: Formal analysis (equal); Investigation (equal); Writing – review & editing (equal). **Fabian Kammerbauer**: Methodology (equal); Resources (equal); Writing – review & editing (equal). **Robert Frömter**: Methodology (equal); Resources (equal); Writing – review & editing (equal). **Mathias Kläui**: Funding acquisition (equal); Project administration (equal); Resources (lead); Writing – review & editing (equal). **Dmitry Kozodaev**: Methodology (equal); Resources (equal); Writing – review & editing (equal). **Johan H. Mentink**: Formal analysis (equal); Funding acquisition (lead); Investigation (equal); Project administration (equal); Supervision (equal); Writing – review & editing (equal). **Dmytro Afanasiev**: Formal analysis (equal); Funding acquisition (equal); Investigation (equal); Methodology (equal); Project administration (equal); Supervision (equal); Writing – review & editing (equal). **Theo Rasing**: Conceptualization (equal); Funding acquisition (lead); Investigation (equal); Methodology (equal); Project administration (equal); Supervision

(equal); Writing – review & editing (equal). **Alexey Kimel**: Conceptualization (lead); Funding acquisition (lead); Investigation (equal); Project administration (lead); Resources (equal); Supervision (lead); Writing – original draft (equal); Writing – review & editing (equal).

DATA AVAILABILITY

The data that support the findings of this study are openly available at https://doi.org/10.34973/98w0-ee37. All other data that support the findings of this paper are available from the corresponding author upon reasonable request.

REFERENCES

[1] E. Beaurepaire, J.-C. Merle, A. Daunois, and J.-Y. Bigot, "Ultrafast spin dynamics in ferromagnetic nickel," Phys. Rev. Lett. **76**, 4250–4253 (1996).

[2] J.-Y. Bigot, M. Vomir, and E. Beaurepaire, "Coherent ultrafast magnetism induced by femtosecond laser pulses," Nat. Phys. **5**, 515–520 (2009).

[3] A. Kirilyuk, A. V. Kimel, and T. Rasing, "Ultrafast optical manipulation of magnetic order," Rev. Mod. Phys. **82**, 2731–2784 (2010).

[4] M. Strungaru, S. Ruta, R. F. L. Evans, J. Barker, K. Yuanmae, J. Chureemart, P. Chureemart, T. Rasing, and R. W. Chantrell, "All-optical switching: A path to recording technology beyond HAMR," IEEE Trans. Magn. **61**, 1–9 (2025).

[5] S. Eisebitt, J. Lüning, W. F. Schlotter, M. Lörgen, O. Hellwig, W. Eberhardt, and J. Stöhr, "Lensless imaging of magnetic nanostructures by x-ray spectro-holography," Nature **432**, 885–888 (2004).

[6] B. Pfau, S. Schaffert, L. Müller, C. Gutt, A. Al-Shemmary, F. Büttner, R. Delaunay, S. Düsterer, S. Flewett, R. Frömter, J. Geilhufe, E. Guehrs, C. M. Günther, R. Hawaldar, M. Hille, N. Jaouen, A. Kobs, K. Li, J. Mohanty, H. Redlin, W. F. Schlotter, D. Stickler, R. Treusch, B. Vodungbo, M. Kläui, H. P. Oepen, J. Lüning, G. Grübel, and S. Eisebitt, "Ultrafast optical demagnetization manipulates nanoscale spin structure in domain walls," Nat. Commun. **3**, 1100 (2012).

[7] C. D. Stanciu, F. Hansteen, A. V. Kimel, A. Kirilyuk, A. Tsukamoto, A. Itoh, and T. Rasing, "All-optical magnetic recording with circularly polarized light," Phys. Rev. Lett. **99**, 047601 (2007).

[8] I. Radu, K. Vahaplar, C. Stamm, T. Kachel, N. Pontius, H. A. Dürr, T. A. Ostler, J. Barker, R. F. L. Evans, R. W. Chantrell, A. Tsukamoto, A. Itoh, A. Kirilyuk, T. Rasing, and A. V. Kimel, "Transient ferromagnetic-like state mediating ultrafast reversal of anti-ferromagnetically coupled spins," Nature **472**, 205–208 (2011).

[9] T. A. Ostler, J. Barker, R. F. L. Evans, R. W. Chantrell, U. Atxitia, O. Chubykalo-Fesenko, S. El Moussaoui, L. Le Guyader, E. Mengotti, L. J. Heyderman, F. Nolting, A. Tsukamoto, A. Itoh, D. Afanasiev, B. A. Ivanov, A. M. Kalashnikova, K. Vahaplar, J. Mentink, A. Kirilyuk, T. Rasing, and A. V. Kimel, "Ultrafast heating as a sufficient stimulus for magnetization reversal in a ferrimagnet," Nat. Commun. **3**, 666 (2012).

[10] R. Medapalli, D. Afanasiev, D. K. Kim, Y. Quessab, S. Manna, S. A. Montoya, A. Kirilyuk, T. Rasing, A. V. Kimel, and E. E. Fullerton, "Multiscale dynamics of helicity-dependent all-optical magnetization reversal in ferromagnetic Co/Pt multilayers," Phys. Rev. B **96**, 224421 (2017).

[11] U. Parlak, R. Adam, D. E. Bürgler, S. Gang, and C. M. Schneider, "Optically induced magnetization reversal in [Co/Pt] multilayers: Role of domain wall dynamics," Phys. Rev. B **98**, 214443 (2018).

[12] G. Kichin, M. Hehn, J. Gorchon, G. Malinowski, J. Hohlfeld, and S. Mangin, "From Multiple- to single-pulse all-optical helicity-dependent switching in ferromagnetic Co/Pt multilayers," Phys. Rev. Appl. **12**, 024019 (2019).

[13] Y. Peng, D. Salomoni, G. Malinowski, W. Zhang, J. Hohlfeld, L. D. Buda-Prejbeanu, J. Gorchon, M. Vergès, J. X. Lin, D. Lacour, R. C. Sousa, I. L. Prejbeanu, S. Mangin, and M. Hehn, "In-plane reorientation induced single laser pulse magnetization reversal," Nat. Commun. **14**, 5000 (2023).

[14] D. Metternich, K. Litzius, S. Wintz, K. Gerlinger, S. Petz, D. Engel, T. Sidiropoulos, R. Battistelli, F. Steinbach, M. Weigand, S. Wittrock, C. Von Korff Schmising, and F. Büttner, "Defects in magnetic domain walls after single-shot all-optical switching," Struct. Dyn. **12**, 024504 (2025).

[15] D. Khusyainov, R. Liefferink, M. Na, F. Kammerbauer, R. Frömter, M. Kläui, D. Kozodaev, N. Vovk, R. V. Mikhaylovskiy, D. Afanasiev, A. V. Kimel, J. H. Mentink, and T. Rasing, "Texture-dependent all-optical switching in ferromagnetic films via stochastic nucleation of nanoscale domains," Nat. Mater. (published online 2026).

[16] R. Hosseinifar, F. Steinbach, I. Kumberg, J. M. Lendínez, S. Thakur, S. E. Hadjadj, J. Gördes, C. S. Awsaf, M. Fix, M. Albrecht, F. Kronast, U. Atxitia, C. Von Korff Schmising, and W. Kuch, "All-optical magnetization switching of GdFe by double-pulse laser excitation," Phys. Rev. B **112**, 174406 (2025).

[17] F. Steinbach, N. Stetzuhn, D. Engel, U. Atxitia, C. Von Korff Schmising, and S. Eisebitt, "Accelerating double pulse all-optical write/erase cycles in metallic ferrimagnets," Appl. Phys. Lett. **120**, 112406 (2022).

[18] C. Banerjee, K. Rode, G. Atcheson, S. Lenne, P. Stamenov, J. M. D. Coey, and J. Besbas, "Ultrafast double pulse all-optical reswitching of a ferrimagnet," Phys. Rev. Lett. **126**, 177202 (2021).

[19] S. Wang, C. Wei, Y. Feng, H. Cao, W. Li, Y. Cao, B.-O. Guan, A. Tsukamoto, A. Kirilyuk, A. V. Kimel, and X. Li, "Dual-shot dynamics and ultimate frequency of all-optical magnetic recording on GdFeCo," Light: Sci. Appl. **10**, 8 (2021).

[20] K. T. Yamada, A. V. Kimel, K. H. Prabhakara, S. Ruta, T. Li, F. Ando, S. Semin, T. Ono, A. Kirilyuk, and T. Rasing, "Efficient all-optical helicity dependent switching of spins in a Pt/Co/Pt film by a dual-pulse excitation," Front. Nanotechnol. **4**, 765848 (2022).

[21] A. Schwarz and R. Wiesendanger, "Magnetic sensitive force microscopy," Nano Today **3**, 28–39 (2008).

[22] O. Kazakova, R. Puttock, C. Barton, H. Corte-León, M. Jaafar, V. Neu, and A. Asenjo, "Frontiers of magnetic force microscopy," J. Appl. Phys. **125**, 060901 (2019).

[23] T. Noll, D. Engel, T. Sidiropoulos, P. Singh, M. Voigt, D. Sommer, L. Marie-Kern, and S. Eisebitt, "Combined implementation of fs-laser pulses, ns-current pulses, and a bipolar magnetic field in a MFM sample environment," Rev. Sci. Instrum. **96**, 123709 (2025).

[24] T. Sidiropoulos, P. Singh, T. Noll, M. Schneider, D. Engel, D. Sommer, F. Steinbach, I. Will, B. Pfau, C. Von Korff Schmising, and S. Eisebitt, "Subwavelength localized all-optical helicity-independent magnetic switching using plasmonic gold nanostructures," Nano Lett. **25**, 4645–4651 (2025).

[25] C.-H. Lambert, S. Mangin, B. S. D. C. S. Varaprasad, Y. K. Takahashi, M. Hehn, M. Cinchetti, G. Malinowski, K. Hono, Y. Fainman, M. Aeschlimann, and E. E. Fullerton, "All-optical control of ferromagnetic thin films and nanostructures," Science **345**, 1337–1340 (2014).

[26] Y. Quessab, R. Medapalli, M. S. El Hadri, M. Hehn, G. Malinowski, E. E. Fullerton, and S. Mangin, "Helicity-dependent all-optical domain wall motion in ferromagnetic thin films," Phys. Rev. B **97**, 054419 (2018).

[27] K. T. Yamada, S. Ruta, A. V. Kimel, K. H. Prabhakara, T. Li, F. Ando, S. Semin, T. Ono, A. Kirilyuk, R. W. Chantrell, and T. Rasing, "Ultrafast ferromagnetic spin switching by a single pair of optical pulses," IEEE Trans. Magn. **61**, 1–8 (2025).

[28] T. X. Huang, W. Zhang, M. Hehn, G. Malinowski, S. Mangin, and J. Hohlfeld, "Role of domain nucleation and domain wall motion in all-optical helicity-dependent switching," Phys. Rev. B **111**, 144408 (2025).

[29] J. Gorchon, Y. Yang, and J. Bokor, "Model for multishot all-thermal all-optical switching in ferromagnets," Phys. Rev. B **94**, 020409 (2016).

[30] F. Wang, D. E. Bürgler, R. Adam, U. Parlak, D. Cao, C. Greb, S. Heidtfeld, and C. M. Schneider, "Magnetization relaxation dynamics in $[Co/Pt]_3$ multilayers on pico- and nanosecond timescales," Phys. Rev. Res. **3**, 033061 (2021).

[31] B. Koopmans, G. Malinowski, F. Dalla Longa, D. Steiauf, M. Fähnle, T. Roth, M. Cinchetti, and M. Aeschlimann, "Explaining the paradoxical diversity of ultrafast laser-induced demagnetization," Nat. Mater. **9**, 259 (2009).

[32] P. J. Metaxas, J. P. Jamet, A. Mougin, M. Cormier, J. Ferré, V. Baltz, B. Rodmacq, B. Dieny, and R. L. Stamps, "Creep and flow regimes of magnetic domain-wall motion in ultrathin Pt/Co/Pt films with perpendicular anisotropy," Phys. Rev. Lett. **99**, 217208 (2007).

[33] M. J. Dunlavy and D. Venus, "Critical slowing down in the two-dimensional Ising model measured using ferromagnetic ultrathin films," Phys. Rev. B **71**, 144406 (2005).

[34]M. F. Collins, *Magnetic Critical Scattering* (Oxford University Press, Inc, New York, 1989).
[35]X.-X. Zhang, S. Jiang, J. Lee, C. Lee, K. F. Mak, and J. Shan, "Spin dynamics slowdown near the antiferromagnetic critical point in atomically thin $FePS_3$," Nano Lett. **21**, 5045–5052 (2021).
[36]D. Khusyainov, T. Gareev, V. Radovskaia, K. Sampathkumar, S. Acharya, M. Šiškins, S. Mañas-Valero, B. A. Ivanov, E. Coronado, T. Rasing, A. V. Kimel, and D. Afanasiev, "Ultrafast laser-induced spin–lattice dynamics in the van der Waals antiferromagnet $CoPS_3$," APL Mater. **11**, 071104 (2023).
[37]V. A. Drebushchak, "Lambda-peak in heat capacity I. History of the problem," J. Therm. Anal. Calorim. **150**, 15209–15227 (2025).
[38]P. Tengdin, W. You, C. Chen, X. Shi, D. Zusin, Y. Zhang, C. Gentry, A. Blonsky, M. Keller, P. M. Oppeneer, H. C. Kapteyn, Z. Tao, and M. M. Murnane, "Critical behavior within 20 fs drives the out-of-equilibrium laser-induced magnetic phase transition in nickel," Sci. Adv. **4**, eaap9744 (2018).
[39]J.-H. Shim, A. Ali Syed, C.-H. Kim, K. M. Lee, S.-Y. Park, J.-R. Jeong, D.-H. Kim, and D. Eon Kim, "Ultrafast giant magnetic cooling effect in ferromagnetic Co/Pt multilayers," Nat. Commun. **8**, 796 (2017).
[40]L. D. Landau, E. M. Lifshits, and L. P. Pitaevskil, *Statistical Physics* (Pergamon Press, Oxford; New York, 1980).
[41]X. P. Xie, X. W. Zhao, J. W. Knepper, F. Y. Yang, and R. Sooryakumar, "Evolution of magnetic domain reversal with temperature in Co / Pt multilayers observed by magneto-optical Kerr imaging," Phys. Rev. B **76**, 184433 (2007).
[42]F. Büttner, B. Pfau, M. Böttcher, M. Schneider, G. Mercurio, C. M. Günther, P. Hessing, C. Klose, A. Wittmann, K. Gerlinger, L.-M. Kern, C. Strüber, C. von Korff Schmising, J. Fuchs, D. Engel, A. Churikova, S. Huang, D. Suzuki, I. Lemesh, M. Huang, L. Caretta, D. Weder, J. H. Gaida, M. Möller, T. R. Harvey, S. Zayko, K. Bagschik, R. Carley, L. Mercadier, J. Schlappa, A. Yaroslavtsev, L. Le Guyarder, N. Gerasimova, A. Scherz, C. Deiter, R. Gort, D. Hickin, J. Zhu, M. Turcato, D. Lomidze, F. Erdinger, A. Castoldi, S. Maffessanti, M. Porro, A. Samartsev, J. Sinova, C. Ropers, J. H. Mentink, B. Dupé, G. S. D. Beach, and S. Eisebitt, "Observation of fluctuation-mediated picosecond nucleation of a topological phase," Nat. Mater. **20**, 30–37 (2021).
[43]M. C. H. Jong, D. Khusyainov, J. Hintermayr, B. Sanders, D. Kozodaev, A. V. Kimel, B. Koopmans, T. H. M. Rasing, and R. Lavrijsen, "Facilitating electrical and laser-induced skyrmion nucleation with a dipolar-field enhanced effective DMI," arXiv:2602.01818 (2026).
[44]M. Bhukta, T. Dohi, V. K. Bharadwaj, R. Zarzuela, M.-A. Syskaki, M. Foerster, M. A. Niño, J. Sinova, R. Frömter, and M. Kläui, "Homochiral antiferromagnetic merons, antimerons, and bimerons realized in synthetic antiferromagnets," Nat. Commun. **15**, 1641 (2024).